Optimal digital color image correlation

J Curt, M Capaldo, François Hild, Stéphane Roux

Optimal digital color image correlation

J. CURT[a,b], M. CAPALDO[a], F. HILD[b], S. ROUX [b]

[a] EDF R&D, Dept. ERMES, 7 Boulevard Gaspard Monge, 91120 Palaiseau, France

Email: {jordan.curt, matteo.capaldo}@edf.fr

[b] LMT, ENS Paris-Saclay / CNRS / Université Paris-Saclay

61 Avenue du Président Wilson, 94235 Cachan, France

Email: {francois.hild, stephane.roux}@ens-paris-saclay.fr

Abstract

Within the context of Digital Image Correlation (DIC), the *optimal* treatment of color images is considered. The mathematical bases of a weighted 3-field image correlation are first introduced, which are relevant for RGB encoded images. In this framework, noise characterization methods are developed as noise properties dictate the best suited metric to compare images. Consistent ways to process an image from elementary Bayer matrices are derived. Last, a case study on uncertainty quantification is performed.

Keywords: Digital image correlation, color images, uncertainty quantification

1 Introduction

The analysis of displacement fields of structures during mechanical tests is a key element for validating and identifying numerical models. One of the most commonly used methods to measure displacements is Digital Image Correlation (DIC [1, 2]), which gives access to full-fields. These displacement fields may be sought on various kinematic bases [3], which can be tailored to the underlying mechanics of the problem. Thus, this method can be used to perform complex measurements with a priori knowledge of the phenomena to be accounted for (*e.g.,* crack initiation and propagation [4]).

For scientific applications, monochrome cameras are used in most cases [1]. At each pixel of the sensor, a brightness level is recorded. In standard laboratory conditions, a speckle pattern consisting of black and white paints is applied on the studied surface, which makes the use

of monochrome cameras sufficient. Since the use of these cameras is mostly restricted to the scientific world, the diversity of the cameras available on the market is limited. Conversely, digital color cameras are widely distributed among the public with a large range of choices. High-quality and high-definition color cameras are today available at low cost compared to scientific cameras. It is therefore legitimate to question the best use of their performance. In the literature, digital color cameras have been used for various applications such as modal measurements [5], 3D shape deformation detection [6, 7], hybrid stereocorrelation using infrared and visible light cameras [8, 9]. In these works the interest of using a color camera was not always addressed. The resulting color fields were transformed into a single grayscale field (generally without specifying the transformation used).

From this amount of (color) data, different options are available to perform DIC analyses. One easy choice consists in combining the color information into a single, or "gray," equivalent level, and further use a classical DIC methodology [5]. Generally, the color fields (*i.e.,* single gray level field transition) is not even mentioned in publications. Alternatively, the three color fields (for RGB color encoding) can be exploited [10]. It will depend on the data quality and diversity available from the image. For a gray scale image, the data stored on the three color filters are similar. Thus, performing DIC with only one channel can be considered sufficient. Yet some information is lost, and hence this treatment cannot be "optimal." For colored structures, working with all color components may benefit from all the stored data. However, particular attention must be paid to the noise features of each color.

Many standard color cameras are equipped with the so-called Color Filter Array (CFA) technology. It is assumed that the color fields are continuous and mostly smooth. Thus, the color components are not acquired at every pixel location; they are sampled on a regular array. At each pixel location, a single color component is stored, whereas other ones are calculated thanks to interpolation schemes from neighboring pixels. One of the most utilized architecture is known as the Bayer pattern [11], which ensures to mimic the physiology of the human eye. There are twice as many green elements as red or blue are used to fit with human retina sensor features.

Recent publications have addressed the question of usefulness of color cameras for DIC applications [12, 10, 13]. The influence of several parameters was studied in the literature regarding the use of commercial color cameras, namely, the utility of a color speckle, the demosaicing

algorithm used and the transformation of color fields (from three fields into a single grayscale field).

More remotely related to color, let us mention the case of DIC performed on electron backscattered diffraction (EBSD) maps. In such a case, at each pixel, a crystal orientation information is available, or equivalently, three Euler angles, which can be loosely compared to the three primary colors. However, dealing with crystal orientations, the notion of "distance" between two crystal orientations has an objective meaning, that can easily be handled with a quaternion formalism, leading to an extension of DIC to register EBSD maps as proposed in Ref. [14]. Similarly, the "distance" between two RGB images at corresponding pixels has to be defined for digital color image correlation.

Since the beginning of imaging, the definition of color metrics has been the subject of intense research. For instance, the CIE 1931 color spaces [15, 16] were the first quantitative links between distributions of wavelengths in the electromagnetic visible spectrum, and physiologically perceived colors in human vision. Nowadays, these metrics aim to more accurately represent the perceptions of color differences in the human eye in order to develop the most effective sensors and filters for digital color cameras [17, 18, 19]. For color- DIC, such considerations of human perception have no legitimacy. Instead, it is here proposed to use noise as dictating the most appropriate metric.

The objective of this work is to introduce the mathematical foundations of an optimal DIC method when color cameras are used. The quantification of acquisition noise, which is intrinsic to the camera, is carried out, thereby leading to a unique (*i.e.,* optimal) procedure to compare the distance between images, a question that lies at the root of any DIC formulation. When spatial correlations are present, it will be shown that an appropriate linear transformation at a pre-processing stage can be used to unravel those correlations and restore a uniform white noise for which the comparison metric is trivial. A case study of displacement uncertainty quantification is performed when comparing different color image transformations.

2 DIC

This part aims to present the mathematical framework of optimal color DIC. In the following, a *global*-DIC framework will be used, where the entire Region of Interest, ROI, is considered at once with a finite element discretization of the displacement field. However, this choice has

no consequence on the handling of colors as discussed hereafter. For *local*-DIC, it suffices to consider that what is mentioned for the entire ROI holds for smaller interrogation windows (*e.g.,* "subsets").

2.1 Monochrome DIC

First, DIC with monochrome images is based on registering an image $f(\mathbf{x})$ defined as a "gray" level f for all pixels in a region of interest $\mathbf{x} = [x, y]$ in the reference configuration, and a series of pictures $g(\mathbf{x})$ of deformed configurations. The objective is to measure the displacement field $\mathbf{u}$ that obeys the brightness conservation up to the presence of noise η

$$f(\mathbf{x}) = g(\mathbf{x} + \mathbf{u}(\mathbf{x})) + \eta(\mathbf{x}) \tag{1}$$

In other words, the two images are said to be registered when their difference, the so-called residual, $\rho(\mathbf{x}) = g(\mathbf{x} + \mathbf{u}(\mathbf{x})) - f(\mathbf{x})$, cannot be distinguished from noise.

It is quite usual to face a white Gaussian noise. Gaussian refers to the probability distribution function that is a centered Gaussian, and thus only characterized by its standard deviation $\sigma(\mathbf{x})$. "White" means that the noise affecting two distinct pixels is uncorrelated, so that the power spectrum of the pair correlation function is uniform over all wavevectors, akin to "white light," which has a uniform power density over all wavelengths. It is worth noting that noise usually affects both reference and deformed images. However, when both noise fields are uncorrelated, they can be grouped as one equivalent field as above written, with a double variance as compared to each single-image noise field.

In the case of white and Gaussian noise, the probability of observing a residual $\rho(\mathbf{x})$ at point $\mathbf{x}$ reads

$$P(\rho(\mathbf{x})) = \frac{1}{\sigma(\mathbf{x})\sqrt{2\pi}} \exp\left(-\frac{\rho(\mathbf{x})^2}{2\sigma(\mathbf{x})^2}\right) \tag{2}$$

If η is "white," the probability of obtaining a residual field $\rho(\mathbf{x})$ over the ROI composed of N_x

pixels is simply the product of the pixel-to-pixel probabilities

$$\begin{aligned} P(\rho) &= \prod_{i=1}^{N_x} P(\rho(\mathbf{x}_i)) \\ &= \prod_{i=1}^{N_x} \frac{1}{\sigma(\mathbf{x}_i)\sqrt{2\pi}} \exp\left(-\frac{\rho(\mathbf{x}_i)^2}{2\sigma(\mathbf{x}_i)^2}\right) \\ &= \left(\prod_{i=1}^{N_x} \frac{1}{\sigma(\mathbf{x}_i)\sqrt{2\pi}}\right) \exp\left(-\sum_{i=1}^{N_x} \frac{\rho(\mathbf{x}_i)^2}{2\sigma(\mathbf{x}_i)^2}\right) \end{aligned} \tag{3}$$

where the products or sums run over all pixel labels i, while $\mathbf{x}_i$ refers to their location. Thus, the maximum likelihood of this residual is achieved by minimizing the opposite of the argument of the exponential, *i.e.,* the quadratic pixel-to-pixel difference between both pictures, weighted by the inverse noise variance

$$\begin{aligned} Q &= \frac{1}{2}\sum_{i=1}^{N_x} \left(\frac{\rho(\mathbf{x}_i)}{\sigma(\mathbf{x}_i)}\right)^2 \\ &= \frac{1}{2}\sum_{i=1}^{N_x} \left(\frac{f(\mathbf{x}_i) - g(\mathbf{x}_i + \mathbf{u}(\mathbf{x}_i))}{\sigma(\mathbf{x}_i)}\right)^2 \end{aligned} \tag{4}$$

Moreover, if the standard deviation of the noise is uniform throughout the considered ROI, the maximum likelihood of image matching reduces to minimizing the quadratic pixel-to-pixel difference

$$Q[\mathbf{u}] = \frac{1}{2\sigma^2}\sum_{i=1}^{N_x} (f(\mathbf{x}_i) - g(\mathbf{x}_i + \mathbf{u}(\mathbf{x}_i)))^2 \tag{5}$$

This derivation proves that when white, Gaussian and uniform noise occurs, then the Euclidean norm of the difference between the reference and the corrected deformed image is *optimal* (*i.e.,* the least sensitive to noise) to register two grayscale images. Any other measurement of the discrepancy between these images may be used successfully. However, the corresponding uncertainty of the result cannot be smaller than with the above objective functional Q.

2.2 Color image registration

A color image is usually composed of three fields for each of the primary hues. The most common technology is the Bayer filter consisting of four primary sensors organized as 2×2 subpixels. Each pixel contains two green, one red and one blue sensors [11]. Figure 1 shows one possible sensor ordering, referred by the initial of the color of the matrix (top-bottom, left-right). These pixels repeat themselves horizontally and vertically.

Figure 1: Bayer pattern that can be used in color cameras

The reconstruction of the color fields on all elementary detectors from the Bayer matrix with the use of *demosaicing* algorithms consists in the interpolation of fields. Generally, the set of three color components is Red, Green and Blue (RGB). The stored data must be post-processed and interpolated [20, 21, 22] to obtain three complete color channel planes. All algorithms aim at enhancing contrasts and restoring human vision. Some works have been devoted to understanding which demosaicing interpolation scheme is better suited for DIC purposes [23, 10]. The main conclusion is that low order interpolation schemes perform better. The algorithm that provides better results in terms of error and uncertainty was the one with no interpolation where the subpixels are *binned*. Only pixels corresponding to a Bayer elementary matrix were considered as a unique gray level pixel [10]. The bias induced by demosaicing results in noise with spatial correlations [6], which is not appropriate for DIC applications [10].

As seen for the previous monochrome case, DIC starts from a distance between two images, namely 1) the reference image and 2) the corrected deformed one, and among many possible distances, the one that is optimal exploits the known statistical information on noise within a Bayesian framework. Thus, it is crucial to characterize noise of color pictures in order to assess whether it may (or not) account for a given image difference.

When no spatial correlations are present, and for a Gaussian noise, the entire statistical characterization is contained in the covariance matrix $\mathbf{C}$ defined as

$$C_{ij} = \langle \eta_i(\mathbf{x}) \eta_j(\mathbf{x}) \rangle \tag{6}$$

where $\eta_i(\mathbf{x})$ is the noise affecting the i-th color channel at pixel $\mathbf{x}$, and $\langle \bullet \rangle$ denotes the statistical expectation. It is assumed that $\langle \eta_i \rangle = 0$, otherwise a bias would be present, and in this case, because it would affect all images in the same way, it would not contribute to image

differences and hence would be harmless.

Based on the color covariance matrix, the probability density for a noise vector $\boldsymbol{\eta}$ reads

$$P(\boldsymbol{\eta}) = \frac{1}{\det(\mathbf{C})(2\pi)^{3/2}} \exp\left(-\frac{1}{2}\boldsymbol{\eta}\mathbf{C}^{-1}\boldsymbol{\eta}\right) \tag{7}$$

Following the same footsteps as in the previous section, it is straightforward to express the probability that a color residual $\rho_i = f_i(\mathbf{x}) - g_i(\mathbf{x}+\mathbf{u}(\mathbf{x}))$ be solely due to noise. Maximizing this probability over trial displacement fields provides the *optimal* variational formulation of color DIC. More precisely, the co-logarithm of the likelihood is to be minimized, or

$$Q_N[\mathbf{u}] = \frac{1}{2}\sum_{k=1}^{N_x}\sum_{i=1}^{3}\sum_{j=1}^{3}\rho_i(\mathbf{x}_k)C_{ij}^{-1}(\mathbf{x}_k)\rho_j(\mathbf{x}_k) \tag{8}$$

where 3 is number of channels, and can be straightforwardly generalized to N if more channels are used (say for hyperspectral imaging).

It can be observed that in the case of a noise that would uniformly affect all three color channels without correlation and with identical variance, then the above functional reduces to the canonical form

$$Q_3[\mathbf{u}] \propto \sum_{k=1}^{N_x}\sum_{i=1}^{3}(f_i(\mathbf{x}) - g_i(\mathbf{x}+\mathbf{u}(\mathbf{x})))^2 \tag{9}$$

3 Noise characterization

In this section, a method for characterizing the intrinsic noise of color cameras is introduced. Three properties are studied, namely, uniformity, spatial correlations and color space correlations. A set of color images with color speckle pattern is considered (Figure 2).

Figure 2: Color speckle pattern used herein

The experiment was very simple. A speckled sheet of paper, placed on a horizontal table, was repeatedly photographed with a camera mounted on a tripod. The hardware parameters of the optical setup are reported in Table 1.

Table 1: DIC hardware parameters

Camera	CANON E70D
Definition	2748×1835 (Bayer) pixels
Color filter	Bayer
Gray Levels amplitude	14 bits (raw data)
Lens	CANON 50-mm
Aperture	$f/12$
Field of view	274×182 mm^2
Image scale	100 µm/pixel
Stand-off distance	30 cm
Image acquisition rate	1-2 fps
Patterning technique	sprayed paints (see more details in text and Figures 2 and 10)
Pattern feature size (B/W)	3.4 pixels
Pattern feature size (colored)	3.8 pixels

The noise of color channel i in image number n, $\eta_i^n(\mathbf{x})$, is obtained from the following steps:

1. After converting all color images to a (monochrome) gray scale thanks to an rgb2gray transform [24, 25], the nth image was registered with the first one accounting for a

rigid translation, $\mathbf{u}^n$. This registration was performed in Fourier space using cross-correlations [26].

2. From the measured displacements, corrected images were computed $\tilde{g}_i^n(\mathbf{x}) = g_i^n(\mathbf{x} + \mathbf{u}^n)$. The chosen subpixel interpolation scheme was cubic (Table 2).

3. An average color reference image, $\hat{f}(\mathbf{x})$ was obtained by averaging over all corrected (*i.e.,* registered) color images, $\hat{f}_i(\mathbf{x}) = \langle \tilde{g}_i^n(\mathbf{x}) \rangle_n$ the three color fields with all corrected images $\tilde{g}^n$.

4. Last, the noise was computed as $\eta_i^n(\mathbf{x}) = \tilde{g}_i^n(\mathbf{x}) - \hat{f}_i^n(\mathbf{x})$.

The first two steps were needed because it was observed that spurious rigid body translations of small amplitudes occurred in the acquisition of image series. This may have been caused by ambient vibrations and a compliant setup, but due to the low frequency of acquisition, the translations appeared random in time. If such motions were not corrected, the apparent noise appeared to have a broader scatter, and a higher spatial correlation at short distances.

Table 2: DIC analysis parameters for rigid body translations

DIC software	Correli 3.0 [27]
Image filtering	None
ZOI size	1000×1000 pixels
Step size	None
Shape function	Constant
Matching criterion	Cross-correlation product
Interpolant	cubic
Displacement noise-floor (x direction)	1.6×10^{-2} pixel
Displacement noise-floor (y direction)	2.4×10^{-2} pixel

3.1 Spatial correlations

Let us recall that the 3-layer description of a color image given at the same pixel location is already a reconstruction, and even if no demosaicing algorithm is used, an interpolation scheme is inherently present at the scale of elementary color sensors, beneath the Bayer matrix scale. It is therefore very important to assess the presence or not of spatial correlations in noise.

For a single field of data, the spatial autocorrelation function reads

$$C(\boldsymbol{\delta}) = \langle \eta(\mathbf{x})\eta(\mathbf{x}+\boldsymbol{\delta})\rangle_{\mathbf{x}} \tag{10}$$

where the expectation value denoted by angular brackets can be substituted by a spatial average over $\mathbf{x}$ for stationary fields.

The dimensionless autocorrelation functions of noise on the field associated with the red color are plotted for two images of the sample. In order to quantify acquisition noise, the images are shifted by translation movements using bi-cubic interpolation in both directions with respect to the first image, corresponding to the FFT-DIC calculation result. The applied rigid body displacements, that have been calculated for two real images, are:

- 0.018 pixel along x, 0.036 pixel along y for the first image.
- 0.056 pixel along x, 0.190 pixel along y for the second image.

The autocorrelation functions are plotted in two dimensions in Figure 3, and in each direction in Figure 4. The larger the translation amplitudes, the more correlated would nearest neighbor pixels be, as a result of the subpixel interpolation scheme. In particular, for half a pixel translation, the interpolated color level weights equally both neighbors (along each dimension). However, for small amplitude translations, the noise keeps its white character.

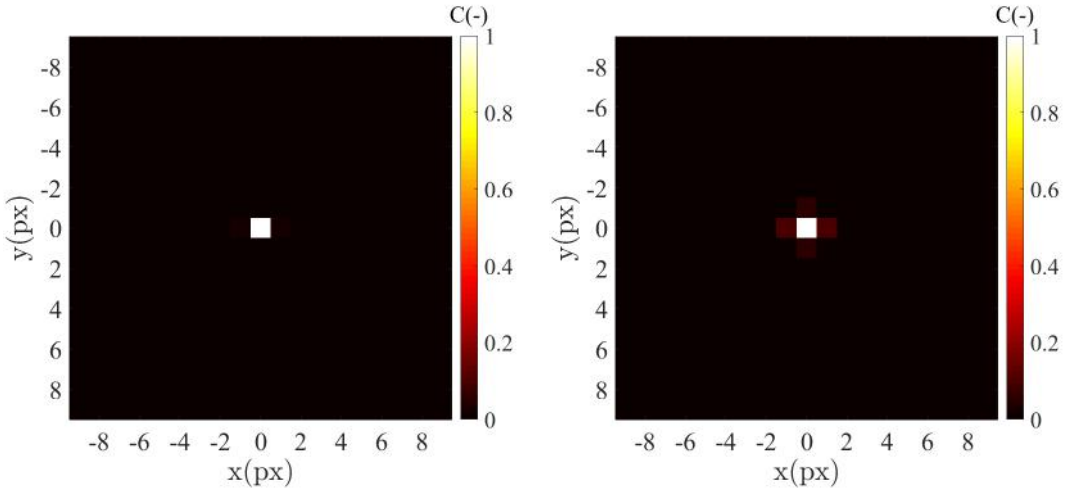

(a) (b)

Figure 3: Autocorrelation functions for the red field for the first (a) and second (b) images

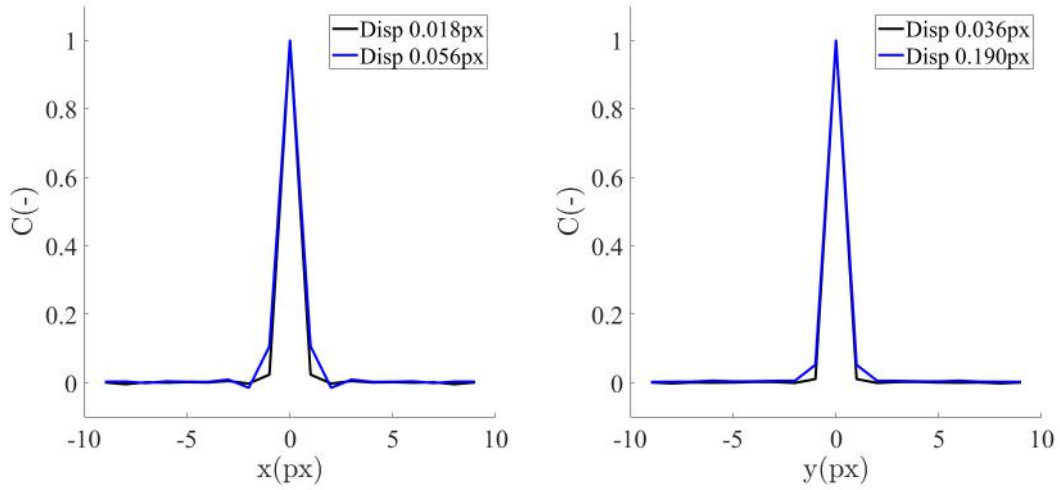

(a) (b)

Figure 4: Autocorrelation functions along x (a) and y (b) directions

3.2 Noise uniformity

To determine the noise amplitude for different brightness levels, pixels are partitioned into 12 classes according to $\hat{f}_i(\mathbf{x})$, the intensity of each color channel of the reference averaged image. The entire encountered brightness range is considered. For each class, the noise variance of $\eta_i^n(\mathbf{x})$ over all pixels $\mathbf{x}$ in the class is calculated for each image n. The latter is plotted as a function of the mean color brightness of the class (for the red channel as an example in Figure 5). Figure 5(b) shows that a much broader data scatter is observed if the slight motion that occurred during image acquisitions is not accounted for.

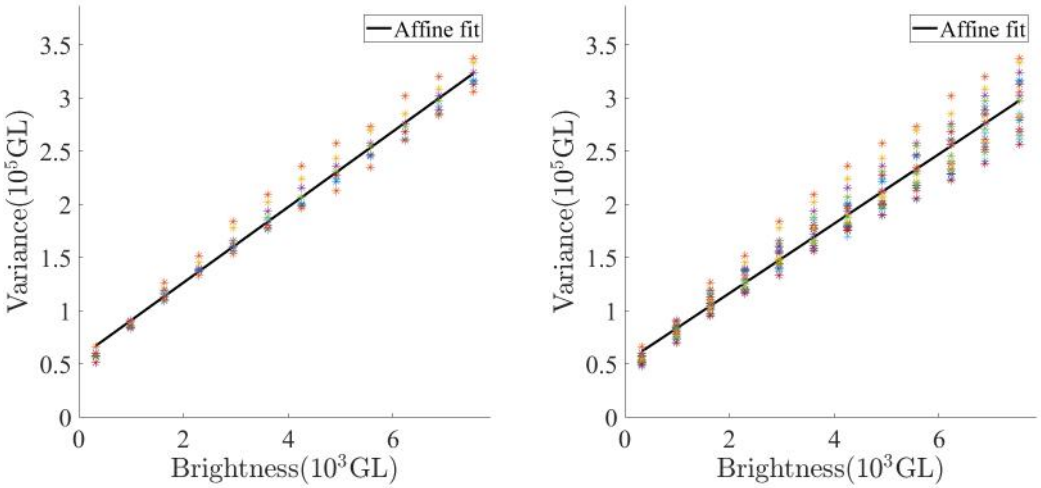

(a) (b)

Figure 5: Variance of red brightness with (a) and without (b) corrections for rigid body motions. Units are in color levels (GL), encoded over 16 bits. The different symbols corresponds to the different images

In Figure 5, an affine regression is also reported, which accounts quite precisely for the data points. This feature is characteristic of Poisson noise, which is a basic form of noise associated with the counting of independent events [28]. Let us note that an offset is introduced here to account for dark field noise. The observed linearity holds also for the other color channels as shown in Figure 6. Let us also underline that the color brightness is always high enough so that the Poisson distribution for the noise distribution matches very accurately a Gaussian distribution.

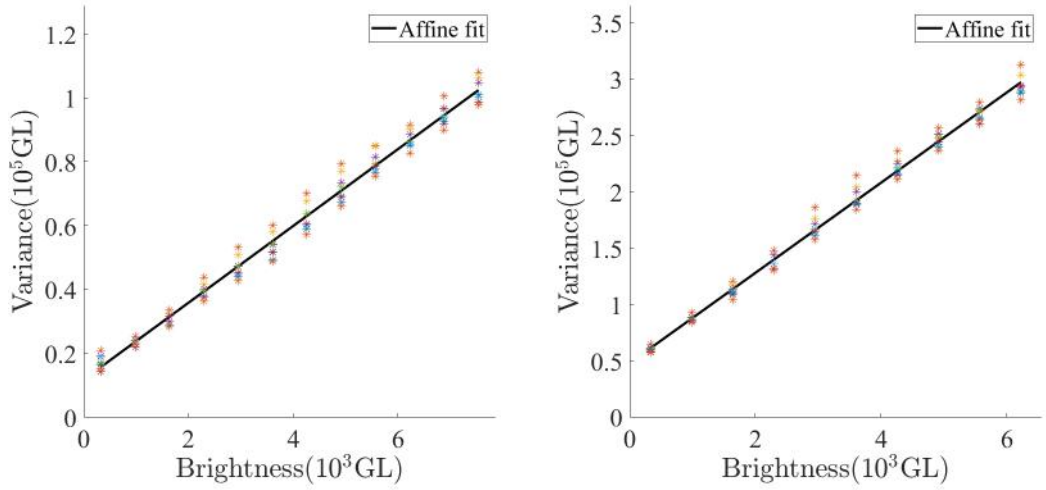

(a) (b)

Figure 6: Variance for the green (a) and blue (b) color fields as functions of the brightness level

To handle images with Poisson noise, which would require a nonuniform weighting for an optimal DIC treatment, it is also possible to have recourse to the Anscombe transform [29, 30], which is a simple nonlinear transform on the brightness that renders the noise variance uniform

$$f_i \longrightarrow \sqrt{f_i - f_{i0}} \tag{11}$$

where f_{i0} corresponds to the offset of the affine regressions shown in Figures 5 and 6. Thus, after a pre-processing step consisting of the Anscombe transform that re-encodes the brightness, there is no need to weight the residuals non-uniformly, and a plain quadratic difference becomes optimal. Such Anscombe transform is applied to each color channel in the image set. To validate this treatment, a similar characterization of the noise variance after the Anscombe transform is performed. Figure 7 shows that indeed most of the systematic variation of the variance with the brightness has been erased or remains within the scatter of data points.

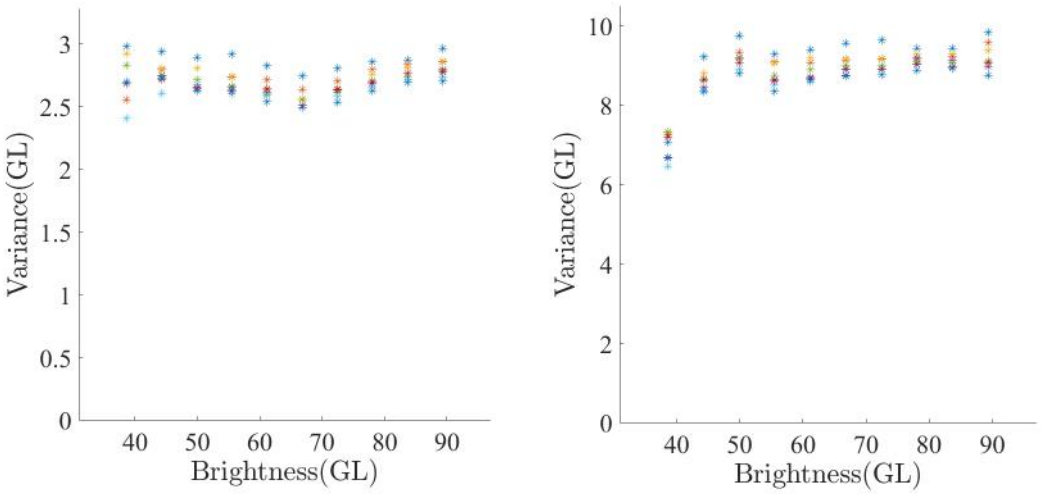

(a) (b)

Figure 7: Variances for the green (a) and blue (b) color fields after Anscombe transform

3.3 Color space correlations

It has been shown, through transformations, that the noise variance can be made uniform with respect to brightness for the three color channels. In addition, if the raw data are used, noise has been shown to be spatially uncorrelated. However, correlations between different color channels after Anscombe transform have not yet been studied. The covariance matrix C (see Equation (6)) is now computed over the entire ROI. This symmetric matrix can be diagonalized, a procedure that allows eigenvectors, *i.e.,* "eigencolors," to be defined as linear combinations of say R, G and B primary colors, which turn out to be uncorrelated. These eigenvectors are shown in Figure 8.

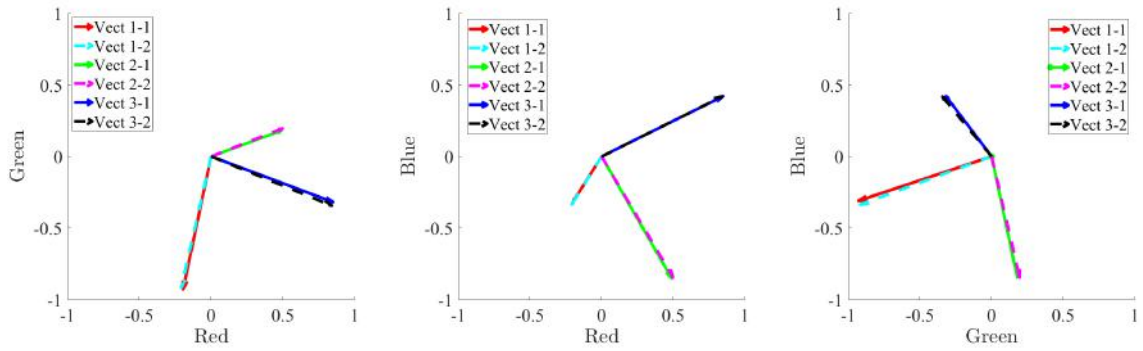

(a) (b) (c)

Figure 8: Plot of noise covariance matrix eigenvectors in planes (a) Red-Green, (b) Red-Blue and (c) Green-Blue. The eigenvector denoted as "Vect $i-j$" corresponds to the ith eigenvector of the jth image

The noise eigenvectors are not oriented along the primary color "directions," thereby revealing that correlations between those primary colors exist. It is noteworthy that the linear transform $\hat{f}_i(\mathbf{x}) = \mathbf{C}_{ij}^{-1/2} f_j(\mathbf{x})$ allows a novel re-encoded image $\hat{f}_i(\mathbf{x})$ to be obtained for which the noise affecting the different color channels i is *independent*, and the noise variance is uniform and equal to 1. To illustrate this last property, Figure 9 shows the three "eigencolors" re-encoding the image displayed in Figure 2.

The procedure that consists in applying the above linear transform, left multiplication of the inverse square root of the covariance matrix, allows the noise affecting the re-encoded quantities to become *perfectly white*. This is very general and can be tailored to a large variety of problems. As a consequence, it renders trivial the handling of a Mahalanobis distance [31], which reduces to a mere Euclidean distance on the re-encoded quantities. The Mahalanobis distance is constructed with the inverse covariance as the metric tensor as in Equation (8). It is the optimal metric in the sense of leading to minimal uncertainties.

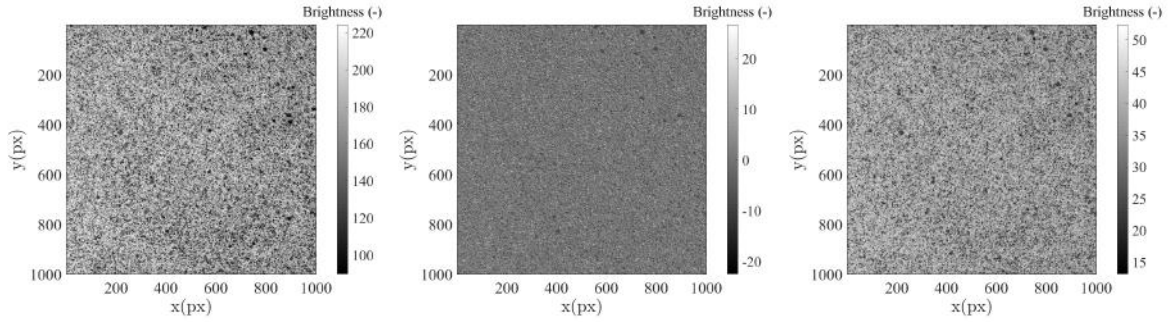

(a) (b) (c)

Figure 9: Projections of Figure 2 onto (a) first, (b) second, and (c) third color modes

It is remarkable that the ranges of intensity of the *new* colors are markedly different due to the fact that noise has now a normalized variance. This method allows the Signal to Noise Ratio (SNR) to be assessed very quickly on each field. The noise intensity is now constant over all the fields. The SNR is only the logarithm of the L2-norm of each $\hat{f}_i$ field. In the present case, the amplitude ranges from 35 to 120 between the three fields.

It is noteworthy that this linear transformation can be applied at the pre-processing stage, after the Anscombe transform. Thus, after this simple color re-encoding (first nonlinear, then linear) the optimal color DIC procedure reduces to the canonical form Q_3 (see Equation (9)), which is mathematically equivalent to Q_N (Equation (8)), using only the Anscombe transformed image, and the full color covariance matrix.

4 Uncertainty quantifications

A way of assessing the noise level and measurement uncertainty is to acquire a set of images of a static sample where the reference image is the first one. This procedure was carried out for two different speckles, namely, one with black and white paints (Figure 10), and another obtained with red-green-blue paints (Figure 2). Let us stress the fact that these two speckles may have slightly different feature sizes (Table 1). However, the important point is not to directly compare them or their results, but rather that the trends obtained with different color processings are similar for both speckles.

Figure 10: Black and white speckle pattern used herein

The same optical setup as previously described was used (Table 1). To evaluate the performance of the DIC algorithm, eight different settings are tested:

- *Monochrome*: correlation with monochrome images issued from direct R-G-B fields summation.
- *Monochrome (rgb2gray)*: correlation with monochrome images issued from R-G-B fields summation with 0.2989, 0.5870, 0.1140 weights. This transform is usually selected to switch from color to grayscale pictures [24, 25].
- *Color*: correlation with color images considering the three color channels independent.
- *Poisson color*: correlation of images on three fields obtained with the Anscombe transform and normalized by their own noise variances.
- *Poisson monochrome*: monochrome images obtained by R-G-B field summation of Anscombe transform and normalization by noise variances in each color channel.
- *Eigencolor modes*: correlation with images projected onto noise eigencolor modes.
- *Eigencolor to monochrome*: monochrome image correlation obtained after summation of the three eigencolor mode fields.

The images were processed using the Correli 3.0 software (Table 3). It corresponds to global DIC with meshes made of 3-noded (T3) elements. When color images are considered, all color layers have the same kinematics. Therefore, all DIC Hessians (*i.e.,* one per color channel) and

all gradients of the DIC cost functions are considered as an overdetermined system to compute the common displacement field, and the latter is used to similarly correct all color layers of the deformed image.

Table 3: DIC analysis parameters

DIC software	Correli 3.0 [27]
Image filtering	see text
Element length	40 pixels
Shape functions	linear (T3)
Mesh	regular
Matching criterion	see text
Interpolant	cubic
Displacement noise-floor	see Figures 11 and 12

For each registration, the standard uncertainty is determined. It corresponds to the standard deviation of all nodal displacements in both directions. The results are shown in Figure 11 (resp. 12) for the black and white (resp. color) speckle pattern. Ten images were selected to show that the reported trends hold for the whole image series.

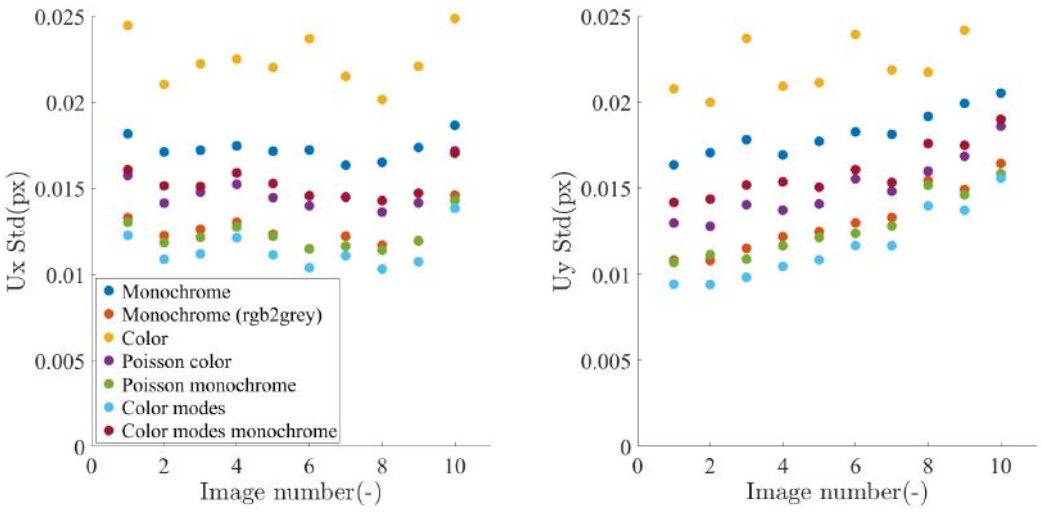

(a) (b)

Figure 11: Standard displacement uncertainties with a black and white speckle pattern along x (a) and y (b) directions

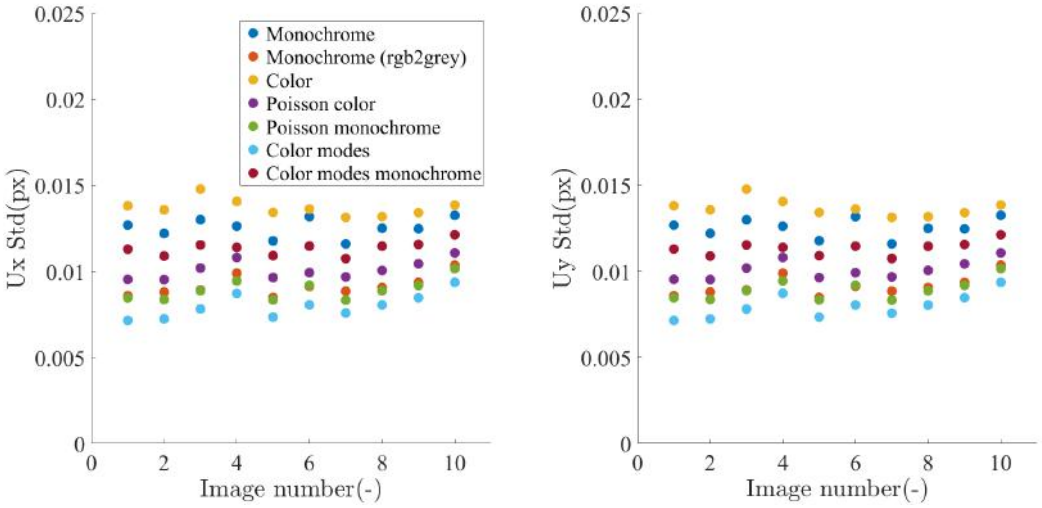

(a) (b)

Figure 12: Standard displacement uncertainties with a color speckle pattern along x (a) and y (b) directions

The general trends are identical for both speckles. First, the highest uncertainties are observed with raw color images (*i.e.,* when the three fields are considered separately with no transform). The measurement uncertainties with monochrome images are lower than when color fields are considered separately with or without performing Anscombe transform and normalization. This observation is not valid when the transform on color modes is considered. The uncertainties are the lowest among all investigated cases. These results show that many different ways of handling color images may be considered, providing all a satisfactory answer, and only their uncertainties allow their respective merit to be ranked. In the above considered examples, the level of uncertainty varies very significantly (by about a factor of two). Among all possible variants, the optimal one (*i.e.,* theoretically defined as leading to the least uncertainty) indeed displays the lowest values.

Last, the uncertainty levels are lower with the colored speckles. These differences may have two causes. First, the combination of speckle and color sensors provides more information and therefore reduces the uncertainties. Second, the density of the colored speckles is higher than that of the black and white speckles (Table 1). No more investigation about this subject was conducted.

5 Conclusion and outlook

In this work, a consistent treatment of noise affecting color images within a Bayesian framework has led to the definition of an optimally-suited metric to evaluate image differences, thereby defining the *optimal* color DIC procedure. Moreover, the above study has shown that the combination of two simple transformations, first an Anscombe transform, followed by a linear color combination along "eigencolors," provided re-encoded images with which the optimal DIC procedure reduces to the canonical form, thereby allowing closed (*e.g.,* commercial) DIC softwares to be used, provided the different layers can be handled.

Quantifications of standard displacement uncertainties were carried out using black and white, as well as color speckles. The conclusions were similar in both cases, namely, the color image transformation for DIC applications had a significant influence on the uncertainty levels (*i.e.,* they can vary by a factor of two). The transformation that allows one to benefit from the lowest uncertainties consists in re-encoding each color intensity using the Anscombe transform, and then further perform a rotation in the color space to align with (appropriately scaled) eigencolors.

The noise characterization was performed on three-color images, which are determined from three filters of different wavelengths. This type of analysis can be extended to hyperspectral image processing, which is much more computationnaly involved, by requiring the noise variance to be uniform and unitary over all processed wavelengths. It enables the whole data set to be reformatted in a canonical form for optimal handling.

Acknowledgements

This work was funded by ANRT and EDF Research and Development.

References

[1] M.A. Sutton, J.J. Orteu, and H. Schreier. *Image correlation for shape, motion and deformation measurements: Basic Concepts, Theory and Applications*. Springer, New York, NY (USA), 2009.

[2] M.A. Sutton. Computer vision-based, noncontacting deformation measurements in mechanics: a generational transformation. *Applied Mechanics Reviews*, 65(5):050802, 2013.

[3] F. Hild and S. Roux. Comparison of local and global approaches to digital image correlation. *Experimental Mechanics*, 52(9):1503–1519, 2012.

[4] S. Roux, J. Réthoré, and F. Hild. Digital image correlation and fracture: an advanced technique for estimating stress intensity factors of 2D and 3D cracks. *Journal of Physics D: Applied Physics*, 42(21):214004, 2009.

[5] C. Jailin. Full field modal measurement with a single standard camera. *Optics and Lasers in Engineering*, 107:265–272, 2018.

[6] L. Yu and B. Pan. Full-frame, high-speed 3D shape and deformation measurements using stereo-digital image correlation and a single color high-speed camera. *Optics and Lasers in Engineering*, 95:17–25, 2017.

[7] L. Yu and B. Pan. Color stereo-digital image correlation method using a single 3CCD color camera. *Experimental Mechanics*, 57(4):649–657, 2017.

[8] A. Charbal, J.-E. Dufour, F. Hild, M. Poncelet, L. Vincent, and S. Roux. Hybrid stereo-correlation using infrared and visible light cameras. *Experimental Mechanics*, 56(5):845–860, 2016.

[9] Y. Wang, A. Charbal, J.-E. Dufour, F. Hild, S. Roux, and L. Vincent. Hybrid multiview correlation for measuring and monitoring thermomechanical fatigue test. *Experimental Mechanics*, DOI: 10.1007/s11340-019-00500-8, 2019.

[10] A. Baldi. Digital image correlation and color cameras. *Experimental Mechanics*, 58(2):315–333, 2018.

[11] B.E. Bayer. Color imaging array. *US patent 3,971,065*, 1976.

[12] D. Hang, G.M. Hassan, C. MacNish, and A. Dyskin. Characteristics of color digital image correlation for deformation measurement in geomechanical structures. In *Digital Image Computing: Techniques and Applications (DICTA), 2016 International Conference on*, pages 1–8. IEEE, 2016.

[13] C. Petiot, S. Roux, and F. Hild. Multi-scale method for emasuring the shape, movement and/or deformation of a structural part subjected to stresses by creating a plurality of

colorimetric speckled patterns. U.S. Patent No. 9,852,514. *Washington, DC: U.S Patent and Trademark Office*, 2015.

[14] Q. Shi, F. Latourte, F. Hild, and S. Roux. Quaternion correlation for tracking crystal motions. *Measurement Science and Technology*, 27(9):095006, 2016.

[15] T. Smith and J. Guild. The CIE colorimetric standards and their use. *Transactions of the optical society*, 33(3):73, 1931.

[16] CIE. Commission internationale de l'éclairage proceedings, 1931. *Cambridge University, Cambridge*, 1932.

[17] T. Indow. Global color metrics and color-appearance systems. *Color Research & Application*, 5(1):5–12, 1980.

[18] M. Melgosa, J.J. Quesada, and E. Hita. Uniformity of some recent color metrics tested with an accurate color-difference tolerance dataset. *Applied Optics*, 33(34):8069–8077, 1994.

[19] N. Ponomarenko, V. Lukin, A. Zelensky, K. Egiazarian, M. Carli, and F. Battisti. Tid2008-a database for evaluation of full-reference visual quality assessment metrics. *Advances of Modern Radioelectronics*, 10(4):30–45, 2009.

[20] P. Longere, X. Zhang, P.B. Delahunt, and D.H. Brainard. Perceptual assessment of demosaicing algorithm performance. *Proceedings of the IEEE*, 90(1):123–132, 2002.

[21] K.-H. Chung and Y.-H. Chan. Color demosaicing using variance of color differences. *IEEE transactions on image processing*, 15(10):2944–2955, 2006.

[22] K. Hirakawa and T.W. Parks. Adaptive homogeneity-directed demosaicing algorithm. *IEEE Transactions on Image Processing*, 14(3):360–369, 2005.

[23] A. Forsey and S. Gungor. Demosaicing images from colour cameras for digital image correlation. *Optics and lasers in engineering*, 86:20–28, 2016.

[24] T. Kumar and K. Verma. A theory based on conversion of rgb image to gray image. *International Journal of Computer Applications*, 7(2):7–10, 2010.

[25] D.J. Higham and N.J. Higham. *MATLAB guide*, volume 150. Siam, 2016.

[26] F. Hild and S. Roux. Digital image correlation. In P. Rastogi and E. Hack, editors, *Optical Methods for Solid Mechanics. A Full-Field Approach*, pages 183–228, Weinheim (Germany), 2012. Wiley-VCH.

[27] H. Leclerc, J. Neggers, F. Mathieu, S. Roux, and F. Hild. Correli 3.0. *Agence pour la Protection des Programmes, Paris*, IDDN.FR.001.520008.000.S.P.2015.000.31500, 2015.

[28] T. Buades, Y. Lou, J.-M. Morel, and Z. Tang. A note on multi-image denoising. In *2009 International Workshop on Local and Non-Local Approximation in Image Processing*, pages 1–15. IEEE, 2009.

[29] F.J. Anscombe. The transformation of poisson, binomial and negative-binomial data. *Biometrika*, 35(3/4):246–254, 1948.

[30] F. Sur and M. Grediac. Sensor noise modeling by stacking pseudo-periodic grid images affected by vibrations. *IEEE Signal Processing Letters*, 21(4):432–436, 2014.

[31] P. C. Mahalanobis. On the generalised distance in statistics. *Proceedings of the National Institute of Sciences of India*, 2(1):49–55, 1936.